

Influence of Twin-screw Processing Conditions on the Mechanical Properties of Biocomposites

V. ALVAREZ,¹ A. IANNONI,² J. M. KENNY² AND A. VÁZQUEZ^{1,*}

¹Research Institute of Material Science and Technology (INTEMA)

Engineering Faculty, National University of Mar del Plata

Argentina, Juan B. Justo 4302 (B7608FDQ) Mar del Plata, Argentina

²Materials Engineering Centre, University of Perugia

Loc. Pentima Bassa 21, Terni, Italy

(Received ...)

ABSTRACT: In order to evaluate the effect of processing conditions, composites of MaterBi-Y matrix with 15 wt% sisal fibers are obtained with different temperature profiles and speeds of rotation of the screw, using a twin-screw extruder. Three different temperature profiles are selected. The speeds of rotation are 25, 60, and 80 rpm. The samples are obtained by compression at 180°C and 700 MPa for 10 min.

The mechanical properties of composites increase when the rotation speed changes from 25 to 60 rpm and then decreases. Fiber breakage increases with rotational speed, but aspect ratio increases to two. Increased modulus with fiber aspect ratio is easily understood because longer fibers carry more tensile loads as a result of increase in transfer length. The decrease in the mechanical properties at a high rotational speed can be due to the degradation of the matrix. The impact properties increase when temperature increases. The decrease in impact properties at temperatures above 185°C can be due to the thermal decomposition of the material.

KEY WORDS: processing, twin-screw, biodegradable, starch, natural fiber, sisal fiber.

INTRODUCTION

BIODEGRADABLE COMPOSITES HAVE interesting properties. Composting at the end of life is an attractive route for the disposal of these abundant polymers [1]. Cellulose fiber is low cost, light in weight, abundant, free from health hazards, and has specific competitive mechanical properties. They do not cause any damage by abrasion to the processing machine, and are recyclable and biodegradable [2–7]. They can be used as excellent reinforcing materials for plastics. These composites made with fibers reinforcing

*Author to whom correspondence should be addressed. E-mail: anvazque@fi.mdp.edu.ar

the matrix have better mechanical properties than those containing nonfibrous fillers [8–10]. Properties of fiber-reinforced composites depend on many factors, such as fiber volume fraction, aspect ratio and orientation, adhesion between fiber and matrix, and stress-transfer efficiency on the interface [11].

Different studies have been carried out using sisal fiber as the reinforcement for thermoplastic matrices and their influence on the mechanical properties [12–16]. When composites are processed by extrusion, shear stresses develop during mixing and extrusion, and these stresses cause fiber damage. The shear stresses generated in the extrusion process are used to disperse the fibers into the polymer and they produce a great reduction in the fiber length and diameter. The extent of fiber breakage depends on the time, temperature, and speed of rotation (SR) [2,12].

The processing conditions can influence the extraction of lignin from the natural fibers and/or promote some chemical or physical modification of components during the mixing process. This effect can result from a higher processing temperature, SR, or time of mixing employed to prepare the composites [12].

The aim of this work is to study the effects of processing conditions on the tensile and impact properties of cellulose derivatives/starch blends matrix-short sisal fiber composites.

EXPERIMENTAL

MaterBi-Y, Novamont, Novara, Italy was used as the matrix. This material is a biodegradable, commercial starch-based polymer, with 40 wt% of cellulose acetate, 40 wt% starch, and 20 wt% processing additives [17]. Brascorda, Brazil supplied short sisal fibers with a mean diameter of $300 \pm 50 \mu\text{m}$ and a fiber of average length around $5.2 \pm 1.6 \text{ mm}$ was cut. Fibers were dried in vacuum-oven at 60°C until constant weight was achieved. Contents of 15 wt% fibers were used for preparing the composites.

To evaluate the effect of the processing conditions, composites with 15 wt% sisal fibers were prepared for different temperature profiles and SR of the screw using a twin-screw extruder – counterrotation twin-screw extruder model MD30 from Bausano Co., Italy. This extruder had a screw diameter of 30 mm with an L/d ratio of 19. Three different temperature profiles were selected and are presented in Table 1. Figure 1 shows the scheme of the extruder and the sections where temperature is measured. Speeds of rotation were 25, 60, and 80 rpm. Residence times for these SR were 80, 35, and 26 s, respectively. The pellets obtained were then compression molded into plaques at 180°C and 700 MPa and rapidly cooled down with running water. In order to release thermal stresses generated during molding, the plaques were annealed in an oven for 1 h at 60°C .

Table 1. Temperature profiles used in the twin-screw extruder.

Profile	Feed						Exit
1	150	155	160	155	160	170	180
2	150	160	170	170	175	180	185
3	150	165	175	175	180	185	190

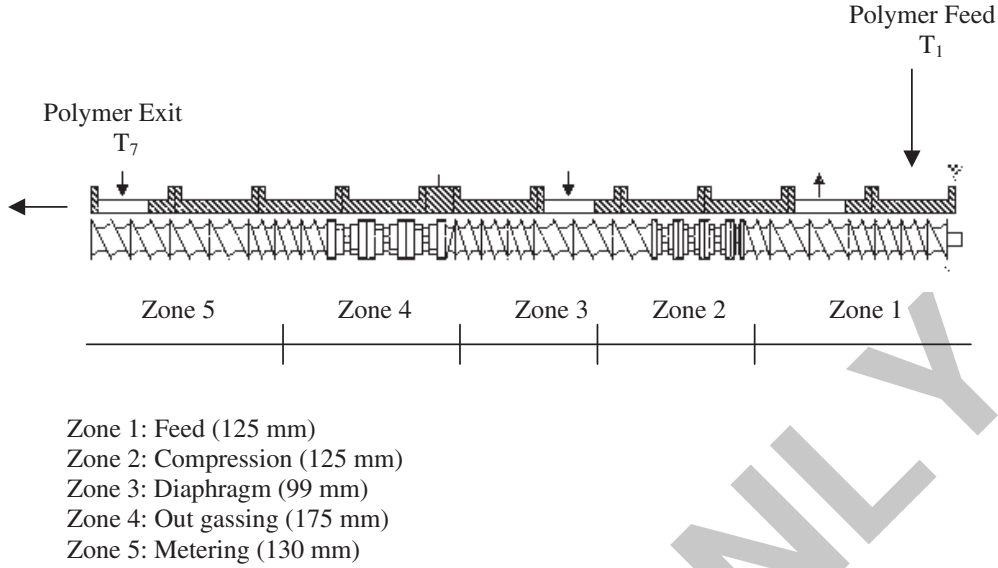


Figure 1. Scheme of the extruder.

Uniaxial tensile tests were carried out on (Type IV ASTM D638-93) dumbbell specimens cut out from compressed plates of 3 mm thickness. The tensile strength and tensile modulus were determined from the maximum and the initial slopes of the true stress–strain curve, respectively.

Tensile tests were performed in an INSTRON 4467 dynamometer with a crosshead speed of 2 mm/min. An incremental mechanical extensometer was used in tensile tests. Mechanical tests were carried out at room temperature.

Out-of-plane fracture toughness of polymers and composites is commonly assessed by the instrumented falling weight impact technique. By this method, the material response against impact loads parallel to the thickness direction can be evaluated [18]. Puncture tests were conducted on samples cut out from compressed plates of 3 mm thickness and 90 mm diameter. These tests were performed in a falling weight Fractovis of Ceast at 1 m/s. The maximum in the load–displacement curves is related to crack initiation. The average load at this point, P_{\max} , was transformed to a stress, which represents the impact strength at crack initiation, σ_d :

$$\sigma_d = 2.5 \cdot \frac{P_{\max}}{t^2} \quad (1)$$

where t is the disk thickness.

The area under the load–displacement curve up to a maximum load represents the energy at crack initiation. Normalizing this value by sample thickness gives:

$$E_{\text{inic}} = \frac{1}{t} \int_0^{x_{\max}} F \cdot dx \quad (2)$$

the total energy required to penetrate the specimen fully, E_{tot} is the total area under the load–displacement curve, also normalized by sample thickness:

$$E_{\text{tot}} = \frac{1}{t} \int_0^{x_{\text{total}}} F \cdot dx \quad (3)$$

The performance against impact perforation of the composites was also evaluated by the ductility index, DI:

$$DI = \frac{E_{\text{prop}}}{E_{\text{total}}} \quad (4)$$

where E_{prop} ($E_{\text{total}} - E_{\text{inic}}$) is the energy required to complete disk penetration after crack initiation, and reflects the post-maximum range.

Dynamic thermogravimetric measurements were performed by using a Shimadzu TGA-DTGA instrument. Temperature programs for dynamic tests were run from 25 to 400°C at a heating rate of 10°C/min. TG/DTG tests were carried out under a nitrogen atmosphere (20 mL/min) in order to prevent any thermoxidative degradation.

The dispersion of fibers in the matrix was observed by optical microscopy. The dispersion of the fibers into the matrix was almost homogeneous except for the composites prepared at the lower temperature profile in which the dispersion was not good enough.

For all processing conditions, fibers were extracted from composites by dissolution of MaterBi-Y matrix using acetone. The fiber diameter and length were measured using an optical microscope OLYMPUS SZH-10.

Effect of Barrel Temperature Profile

The aspect ratio, dispersion, and fiber–matrix interface affect the mechanical properties of short-fiber composites. Fiber length distribution depends, in a very complex manner, on the kind of matrix polymer and its rheological properties, the fiber content, and the resulting interactions. Shear stresses generated in the extruder are very high and can cause the breakdown of the fibers during mixing. Figure 2 shows the fibers after extraction from composites by the dissolution of matrix. The wide distribution of fiber length and diameter are evident in all cases. Fiber defibrillation occurred during the extrusion process, but this effect is more important at higher SR and lower temperature profile. Interfibrillar debonding due to shear and thermal effects should result in a reduction of strength and modulus of the fibers [13]. Breakage pattern can be indicated by fiber length and diameter distribution curves after the extrusion process. Figure 3 shows the fiber length and diameter distributions of composites obtained using different temperature profiles at 60 rpm. The average fiber length (in number and in weight) can be defined as:

$$\bar{L}_n = \frac{\sum N_i \cdot L_i}{\sum N_i} \quad (5a)$$

$$\bar{L}_w = \frac{\sum N_i \cdot L_i^2}{\sum N_i \cdot L_i} \quad (5b)$$

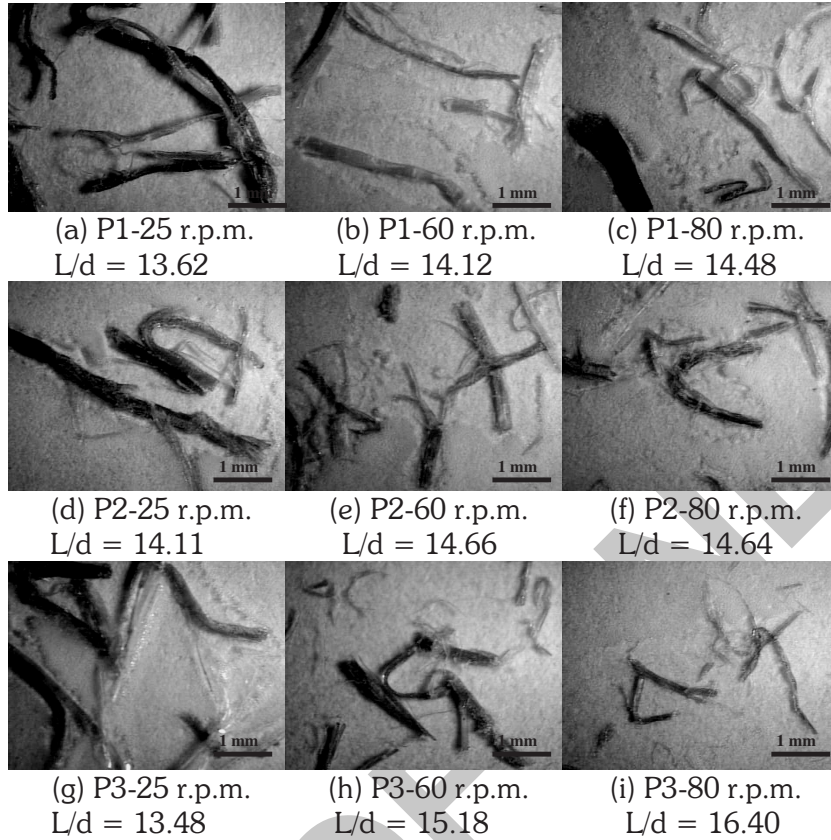


Figure 2. Fiber damage for different temperature profiles: (a) P1-25 rpm; (b) P1-60 rpm; (c) P1-80 rpm; (d) P2-25 rpm; (e) P2-60 rpm; (f) P2-80 rpm; (g) P3-25 rpm; (h) P3-60 rpm; and (i) P3-80 rpm.

where \bar{L}_n is the number-average fiber length, \bar{L}_w is the weight-average fiber length, and N_i is the number of fibers having length L_i . The ratio \bar{L}_w/\bar{L}_n is known as the polydispersity index and can be used as a measure of fiber length distribution [15]. Table 2 shows the average values of fiber dimensions after processing at different temperature profiles and at a SR of 60 rpm.

Figure 4 shows the stress–strain curves obtained by the tensile test for different temperature profiles in the extruder for short-sisal fiber-reinforced MaterBi-Y composites at a SR of 60 rpm.

The nonlinearity observed in these curves can be explained in terms of failure mechanisms operating in fibrous composite materials. The first part of these curves is linear and it reflects the elastic behavior of these materials. The deviation from linear behavior is an indication of the beginning of matrix cracking. The rest of the curve is an indication of the different mechanisms of fiber failure. Sisal fibers are composed of cellulose, hemicellulose, lignin, and pectin [2–4]. Inside the fiber wall, there are many short-aligned microfibrils, which are oriented in a different direction than that of the sisal fiber. Therefore, the wall is a composite structure of lignocellulosic material reinforced with helical microfibrillar bands of cellulose. The microstructure of these fibers is hollow and permits their composites to exhibit different damage and failure mechanisms [18].

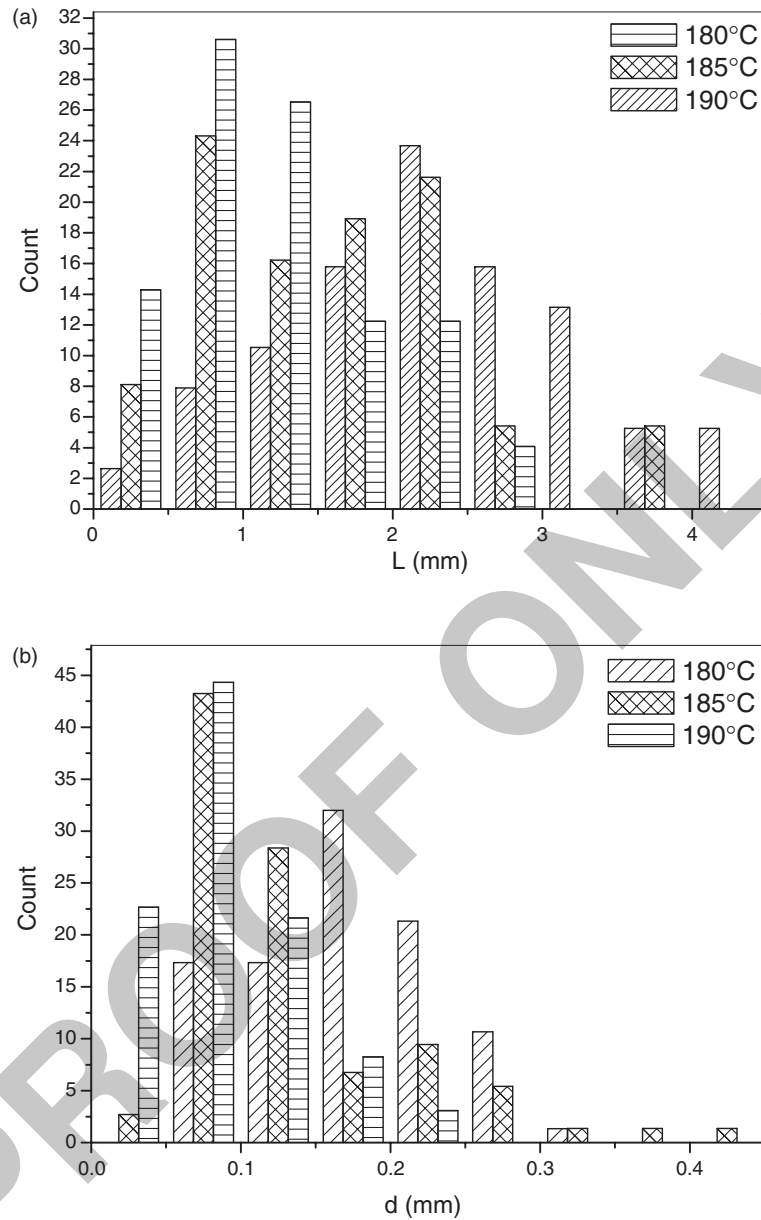


Figure 3. Fiber size distribution for composites obtained using different temperature profiles at 60 rpm: (a) length and (b) diameter.

The failure mechanisms observed in natural fibers are: axial splitting that produces fibrillation, transverse microcracking, and multiple elementary fiber fracture that leads to the fracture of the fiber in the perpendicular direction with respect to the applied load. The macroscopic failure occurs when fiber fracture occurs. The described mechanisms are shown in Figure 5.

Table 2. Average values of fiber dimensions after processing at different temperature profiles and at a speed of rotation of 60 rpm.

Profile	L (mm)	d (mm)	L/d	\bar{L}_n	\bar{L}_w	\bar{L}_w/\bar{L}_n
1	2.23	0.17	14.48	2.23	2.69	1.21
2	1.57	0.13	14.64	1.57	2.06	1.31
3	1.19	0.09	16.40	1.19	1.58	1.33

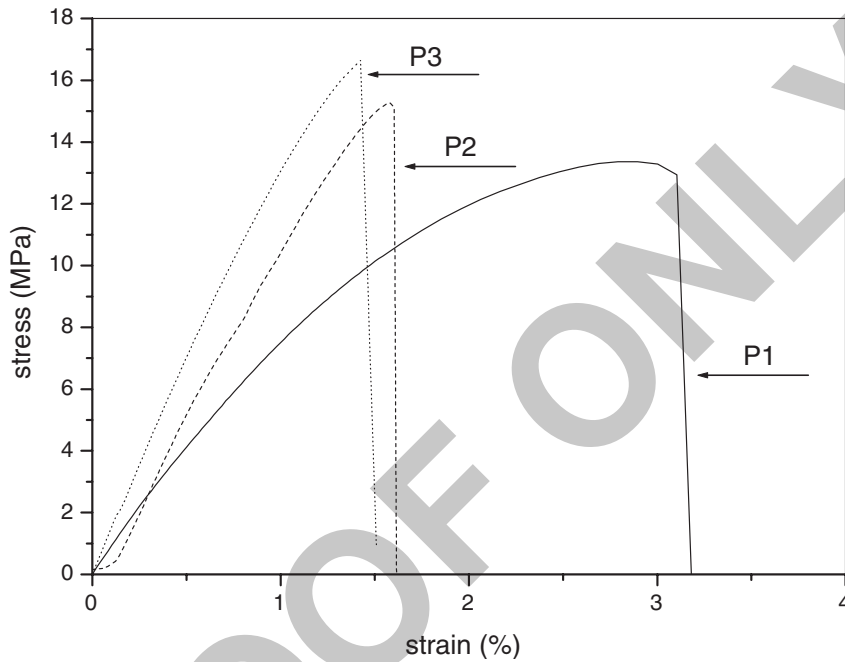
**Figure 4.** True stress–strain curves obtained from tensile tests of composites obtained using different temperature profiles at 60 rpm.

Table 3 shows the effect of the profile of temperature in the extruder on the tensile and impact properties of short sisal fiber-reinforced MaterBi-Y composites at a SR of 60 rpm. The high standard deviations observed in all cases were expected due to the inhomogeneous form of natural fibers and the predominance of defects within their structures. This table shows that the tensile properties (strength and Young's modulus) increase with the rise in temperature. At a lower temperature profile, the mixing is not good enough for the correct dispersion of the fibers into the matrix, hence, the properties of the obtained materials are low. A higher temperature produces a decrease in the viscosity of the matrix and better mixing, but it is also possible that the viscous dissipation increases and the matrix have had some thermal degradation, and the viscosity of the matrix increases due to this effect. Figure 6 shows the micrographs of fracture surface of composite materials extruded at 80 rpm using different temperature profiles. The fracture surfaces of composites have brittle characteristics. The ruptured ends of sisal fibers were not plane, showing some pullout. This is the feature of elementary fiber multicracking followed by interfacial debonding. The fiber–matrix interfacial adhesion

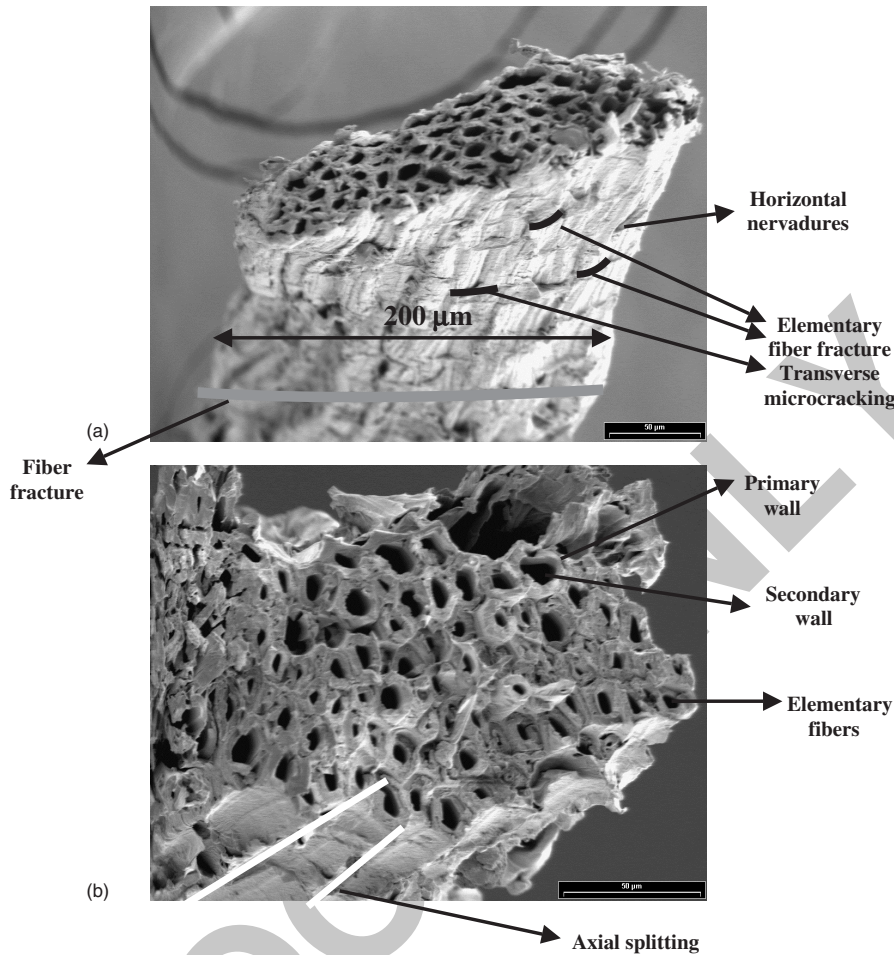


Figure 5. Failure mechanisms observed in sisal fibers.

Table 3. Effect of the profile of temperature in the extruder on the tensile and impact properties of short-sisal fiber-reinforced MaterBi-Y composites at a speed of rotation of 60 rpm.

Profile	Tensile Properties			Impact Properties		
	σ (MPa)	E (GPa)	A (MPa)	σ (MPa)	E (kJ/m)	DI
1	15.2 ± 1.6	0.88 ± 0.08	0.42 ± 0.14	101.0 ± 1.6	0.74 ± 0.01	0.26 ± 0.01
2	16.8 ± 0.9	1.55 ± 0.16	0.12 ± 0.01	134.0 ± 0.9	0.84 ± 0.10	0.68 ± 0.02
3	16.4 ± 1.8	1.60 ± 0.09	0.17 ± 0.05	116.7 ± 1.8	0.82 ± 0.05	0.28 ± 0.02

should be moderate because interfacial debonding can be observed. Decoiling, splitting, and torsion rupture the microcells. It can be observed that some fibers near the fiber–matrix interface, are compressed transversely and, hence, split longitudinally [19]. Figure 6(c) shows the matrix with higher quantity of voids, and a whiter zone close to the

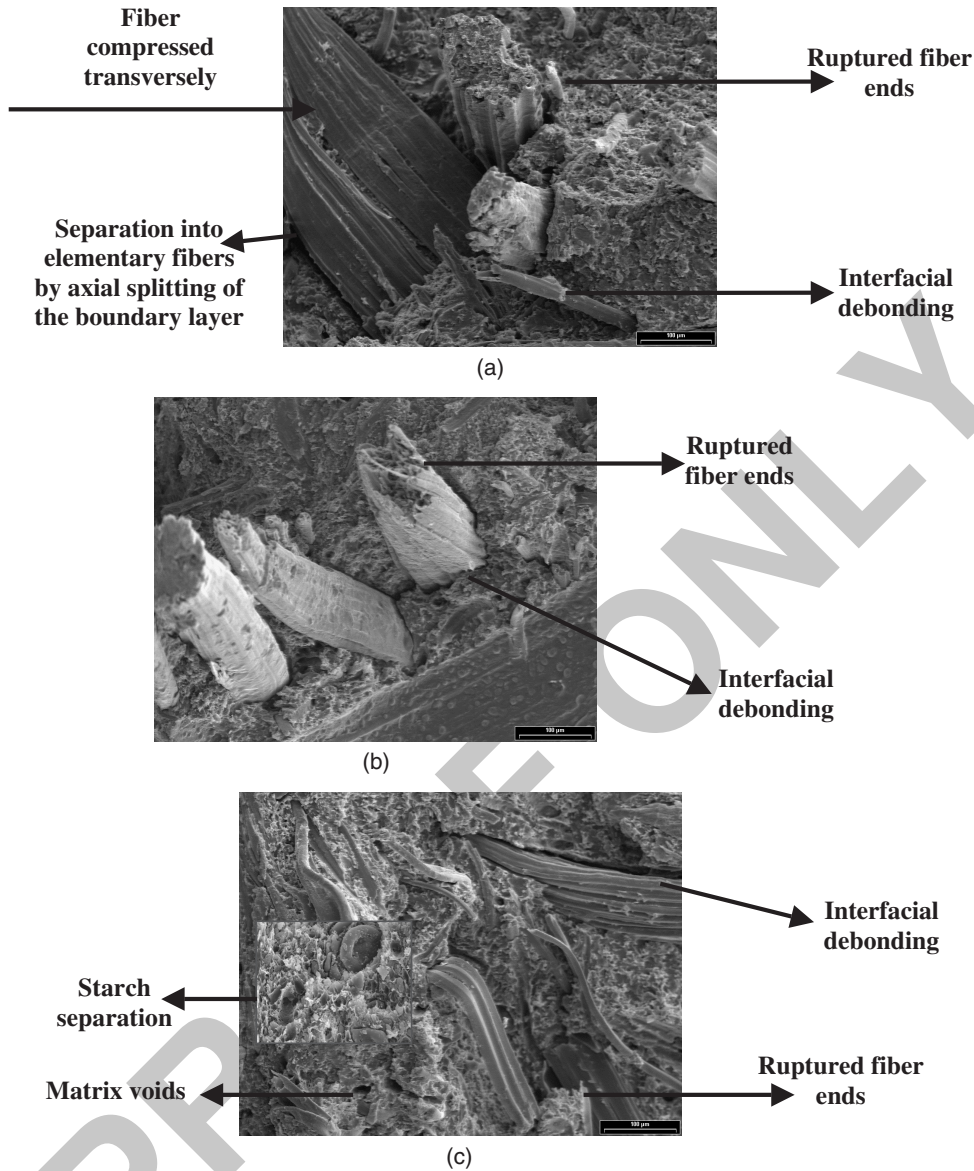


Figure 6. Electron micrograph of composites obtained at 80rpm and at: (a) temperature profile 1; (b) temperature profile 2; and (c) temperature profile 3.

interface, may be due to the starch separation from the matrix and loss of additives of processing. Shear stresses increase due to the increase of viscosity and the fiber aspect ratio also increases. The tensile stress transfer to the fibers increases when the aspect ratio of the fibers increases [3]. From Table 2, it can be seen that the aspect ratio increases when temperature increases leading to higher stress transfer and strength of the composite material.

Toughness of different samples is also presented in Table 3. It can be seen that the lower value was obtained for the second temperature profile with 185°C at the

end of the extrusion. This effect can be explained as a consequence of fiber fibrillation (Figure 6).

(Figures 7 shows the force–displacement curves obtained in puncture tests of composites obtained using different temperature profiles at 60 rpm. The force–deflection curve reflects the associated damage initiated by the first change in the slope of the curve [20]. The peaks on these curves are due to fiber breakage at different times through the striker course. The impact properties obtained from these curves are also presented in Table 3. The decrease of impact properties at temperatures above 185°C can be due to the thermal decomposition of Materbi-Y and sisal fibers. This effect can be observed in Figure 8 from TGA traces. Although thermal degradation can take place at lower temperatures by chain scission, the effect of thermal decomposition on the mechanical properties is higher than that of the chain scission.

It is known [21] that starch and cellulose acetate (MaterBi-Y matrix components) presents a decomposition peak at 320 and at 365°C, respectively. Sisal fibers show two decomposition peaks: one at 300°C (hemicellulose and glycoside unions de-polymerization) and the other at 360°C (thermal degradation of α -cellulose). Lignin presents a broad peak between 200 and 400°C. Alvarez et al. had studied the thermal decomposition of MaterBi-Y–sisal composites determining two decomposition steps: the first one at 300°C had been attributed to the decomposition of lignin, hemicellulose, and starch; and the second one at around 350°C was assigned to the decomposition of cellulose derivatives from MaterBi-Y and cellulose from the sisal fiber [17]. Processing additives are usually compounds of low molecular weight and can be extracted during processing. The higher temperature profile can result in higher starch decomposition and can influence the extraction of lignin from the natural fibers and/or promote some chemical or physical modification of the components during the extrusion process [2,5]. The small holes present

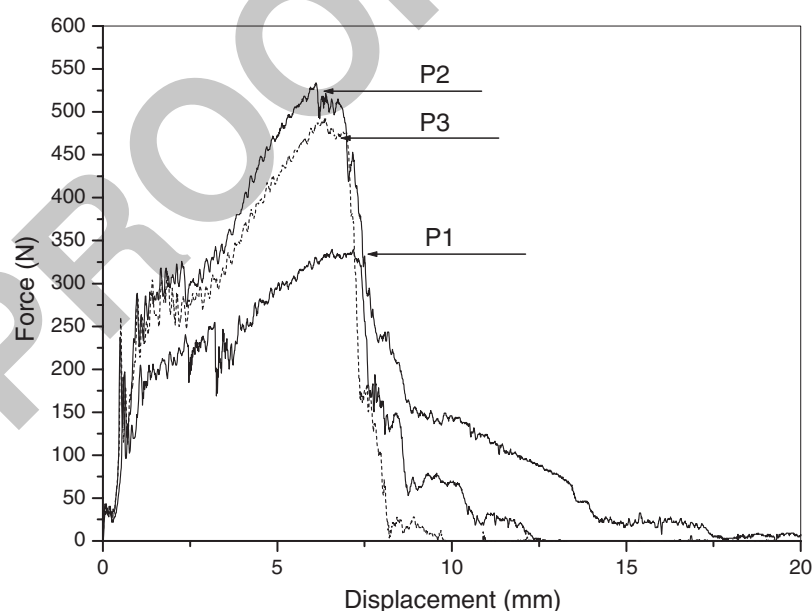


Figure 7. Force–displacement curves obtained in puncture tests of composites obtained using different temperature profiles at 60 rpm.

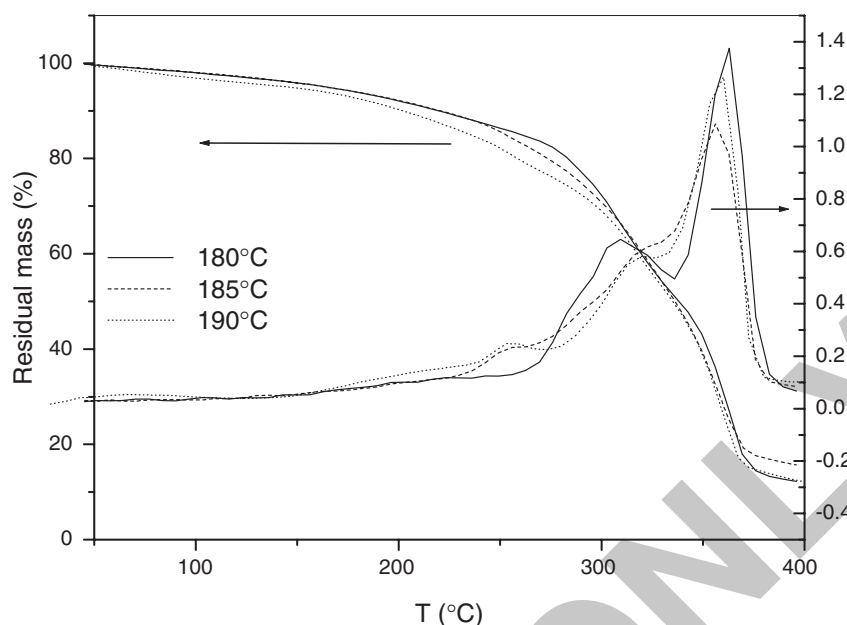


Figure 8. Effect of final temperature in the extruder on the thermal degradation of composites at a speed of rotation of 60 rpm.

in some materials (Figures 6) suggest the presence of porosity induced by the release of bound water or volatile products of fiber and starch decomposition. Lignin extraction could lead to different surface properties of the fibers, which are responsible for the fiber–matrix adhesion.

Effect of Rotation Speed

Several authors [22] determined that shear force in an extruder could cause fiber breakage. It was contended that as the rotational speed increases, the shear forces would increase and the fiber breakage that occurs would be higher, and thus, greater the degree of fiber damage. Figure 9 shows the fiber length and diameter distribution at different SR. The average values of fiber dimensions are shown in Table 4.

Fiber breakage increases with rotational speed, but aspect ratio increases to two. The effect is more important on fiber length than on fiber diameter. In Figure 2, it is possible to observe that fibrillation increases when SR increases.

The stress–strain curves obtained from the tensile test for different SR and the second temperature profile in the extruder are shown in Figure 10. These curves were similar to that obtained at different temperature profiles with an initial linear behavior followed by the nonlinear portion.

Table 5 shows the effect of rotation speed on the mechanical properties of tensile and impact properties of MaterBi-Y composites extrudates at 185°C. For the second temperature profile, the fiber dispersion is better than that for the first one. It can be observed that the mechanical properties of composites increase when SR increases from

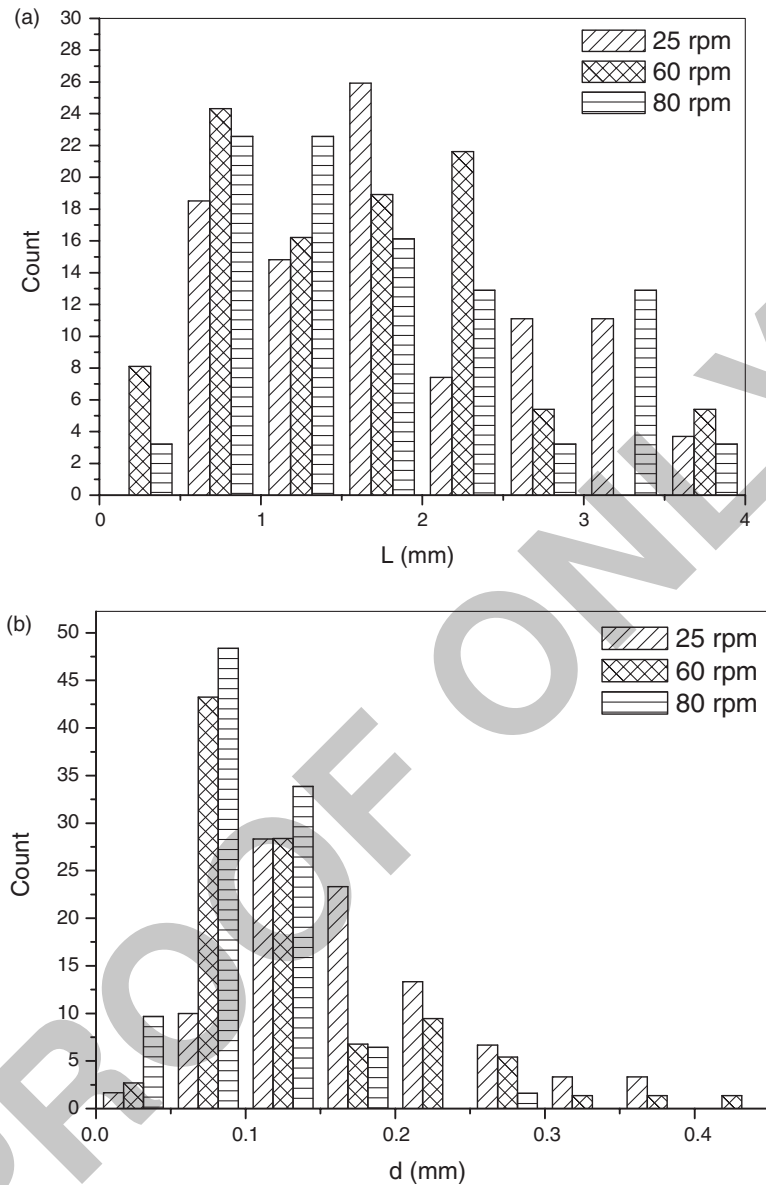
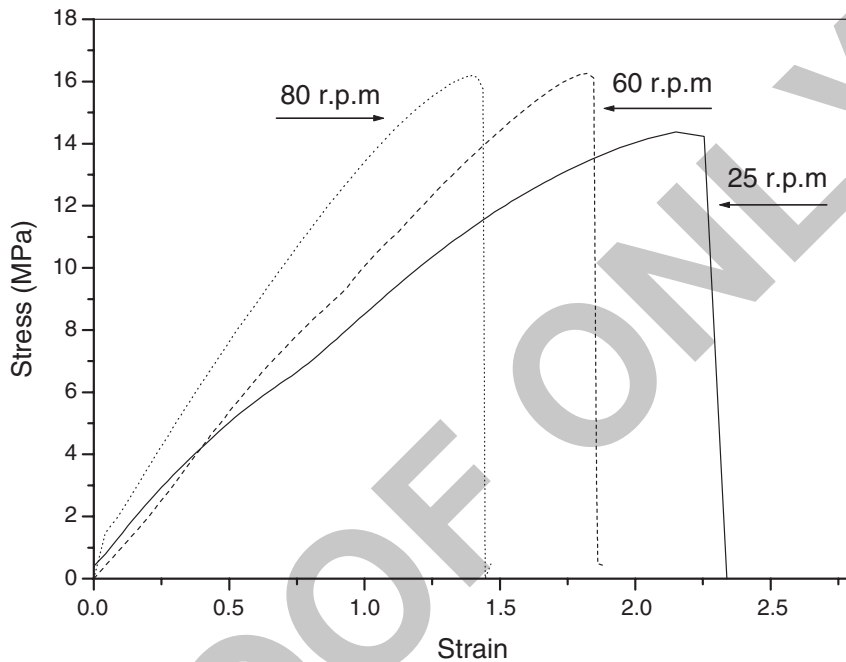


Figure 9. Fiber size distribution for composites obtained using different speeds of rotation at 185°C: (a) length and (b) diameter.

25 to 60 rpm, and then decrease. Increased strength with fiber aspect ratio is easily understood because longer fibers are carrying more tensile loads as a result of increase in transfer length. At high rotational speed, mechanical degradation can occur due to a higher temperature and heat transfer in the barrel, and in spite of the higher aspect ratio of the fibers, the mechanical properties decrease, the impact properties being more sensible to such changes [1]. The low tensile properties observed at a low rotational speed are due to the poor dispersion of sisal fibers in MaterBi-Y matrix. Figure 11 shows the micrograph

Table 4. Average values of fiber dimensions after processing at different rotation speeds using the second temperature profile.

SR	L (mm)	Reduction (%)	d (mm)	Reduction (%)	L/d
25	2.16	58.2	0.173	49.0	13.41
60	1.53	70.4	0.130	57.0	14.66
80	1.47	71.0	0.098	67.3	21.07

**Figure 10.** True stress-strain curves obtained from tensile tests of composites obtained using different speeds of rotation and the second temperature profile.

of composites obtained at the highest temperature profile and at different SR. It can be observed that the collapse of adjacent fibers and local buckling could have a detrimental effect on the mechanical properties of composite materials. The other possible reason is that at a low rotational speed, the fill factor or quantity of polymer into the extruder channel increases and the residence time increases, as a consequence, degradation of the polymer can occur.

At the highest SR, the impact strength of the composite extruded at the lowest temperature (108.8 MPa) is slightly higher than that of the composite extruded at the highest temperature (100.9 MPa). This result can be explained by the degree of heat that the polymer melt suffers due to shear forces generated in the extruder that can degrade the matrix and the natural fibers (by the extraction of lignin), sufficient to affect the impact performance of the composites extruded at higher temperatures [1].

For biocomposites prepared using the lowest temperature profile, the effects of higher SR can make the material more homogenous, thus allowing the composite to have a higher impact strength.

Table 5. Effect of the rotation speed on the extruder on the tensile and impact properties of short-sisal fiber-reinforced MaterBi-Y composites using the second temperature profile.

SR	Tensile Properties		Impact Properties	
	σ (MPa)	E (GPa)	σ (MPa)	E (kJ/m)
25	14.8 ± 1.1	1.17 ± 0.16	130.2 ± 0.6	0.68 ± 0.01
60	16.8 ± 0.9	1.55 ± 0.16	134.0 ± 0.9	0.84 ± 0.10
80	16.1 ± 1.5	1.44 ± 0.10	128.8 ± 1.2	0.74 ± 0.04

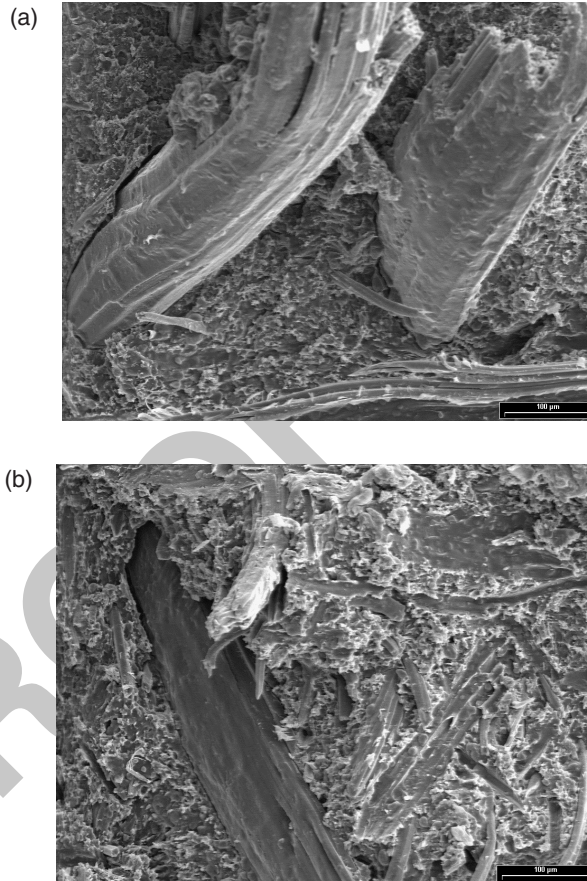


Figure 11. Electron micrograph of composites obtained using temperature profile 3 at different speeds of rotation: (a) 25 rpm and (b) 60 rpm.

CONCLUSIONS

The effect of the processing conditions on the mechanical behavior of MaterBi-Y matrix with 15 wt% sisal fiber composites was studied.

It was demonstrated that both temperature profile and SR, produce fiber damage, especially breakage resulting in fiber length reduction and fibrillation that lead to fiber diameter reduction. Fiber damage increased as SR increased due to the higher shear stresses generated in the extruder. Interfibrillar debonding due to shear and thermal effects not only affect fiber dimensions but also can lead to fibers with reduced strength and modulus.

Irrespective of the SR and the temperature profile used, the stress–strain curves obtained in the tensile test showed an initial linear part followed by a nonlinear part which could be explained by the failure mechanism operating in composite materials. From scanning electron micrographs it was possible to determine these mechanisms: fiber pullout, fiber–matrix debonding, separation of sisal fibers into elementary fibers by axial splitting of the boundary layer, and microcracking of elementary fibers (Figure 5(d)) were observed.

For a fixed SR, mechanical properties increased when temperature increased due to the better fiber distribution of the obtained composite. At the highest temperature, some thermal degradation of matrix (starch) and fibers (lignin extraction) can take place. This result was confirmed by TGA and SEM techniques. Polymer degradation could lead to a material with a higher void content that affects mechanical properties. Lignin extraction affects the fiber surface, which is directly related with fiber–matrix adhesion.

For a fixed temperature profile, mechanical properties of composites increased till a maximum value, and then decreased. At a higher rotational speed, mechanical degradation took place due to a higher heat transfer in the barrel and in spite of the higher aspect ratio of the fibers, the mechanical properties decreased, the impact properties being more sensible to such changes. The low tensile properties observed at low rotation speed were due to the poor dispersion of sisal fibers in MaterBi-Y matrix.

ACKNOWLEDGMENT

Vera Alvarez would like to acknowledge the financial support of Fundación Antorchas. National Research Council (CONICET). Secretaría de Ciencia, Tecnología e Innovación Productiva (SECYT) is also acknowledged for the financial support (PICT12-08011).

REFERENCES

1. Mark Johnson, R., Ticker, N. and Barnes, S. (2003). *Polymer Testing*, **22**: 209.
2. Joseph, P.V., Joseph, K. and Thomas, S. (1999). *Composites Science and Technology*, **59**: 1625.
3. Thwe, M.M and Liao, K. (2003). *Composites Science and Technology*, **63**: 375.
4. Mohanty, A.K., Wibowo, A., Misra, M. and Drzal, L.T. (2004). *Composites Part A*, **35**: 363.
5. Ali, R., Iannace, S. and Nicolais, L. (2003). *Journal of Applied Polymer Science*, **88**: 1637.
6. Oksman, K., Skrifvars, M. and Selin, J.-F. (2003). *Composites Science and Technology*, **63**: 1317.
7. Lundquist, L., Marque, B., Hagstrand, P.-O., Leterrier, Y. and Manson, A.-E. (2003). *Composites Science and Technology*, **63**: 137.
8. Pavithran, C., Mukhrejee, P.S., Brahmakumar, M. and Damodaran, A.D. (1987). *Journal of Material Science Letter*, **6**: 822.
9. White, N.-M. and Ansell, M.P. (1983). *Journal of Material Science*, **18**: 1549.

10. Varma, D.S., Varma, V. and Varma, I.K. (1984). *Textile Research Journal*, **54**: 827.
11. Miwa, M., Nakayama, A., Ohsawa, T. and Hasegawa, A. (1979). *Journal of Applied Polymer Science*, **23**: 2957.
12. Iannace, S., Nocilla, L. and Nicolais, L. (1999). *Journal of Applied Polymer Science*, **73**: 585.
13. Joseph, K., Thomas, S., Pavithran, C. and Brahmakumar, M. (1993). *Journal of Applied Polymer Science*, **47**: 1731.
14. Vázquez, A., Cyras, V.P., Kenny, J.M. and Iannace, S. (1999). *12th International Conference on Composites*, Paris, France.
15. Kumar, R.B., Amma, M.L.G. and Thomas, S. (1995). *Journal of Applied Polymer Science*, **58**: 597.
16. Kuruvilla, J. and Thomas, S. (1996). *Polymer*, **37**: 5139.
17. Alvarez, V.A. and Vázquez, A. (2004). *Polymer Degradation and Stability*, **84**: 13.
18. Mouzakis, D.E., Harmis, T. and Karger-Kocsis (2000). *Polymer Composites*, **8**: 167.
19. Bai, S.L., Li, R.K.Y., Wu, L.C.M., Zeng, H.M. and Mai, Y.U. (1998). *Journal of Material Science Letter*, **17**: 1805.
20. Bledzki, A.K. and Faruk, O. (2004). *Composites Science and Technology*, **64**: 693.
21. Nabi-Shabeb, D. and Jog, J.P. (1999). *Advance in Polymer Technology*, **18**(4): 351.
22. English, B., Youngquist, J.A. and Krysik, A.M. (1994). *Cellulosic Polymer*, Chapter 6.

PROOF ONLY